Determining role of Krein signature for three-dimensional Arnold tongues of oscillatory dynamos

Oleg N. Kirillov,[1,*] Uwe Günther,[2,†] and Frank Stefani[2,‡]
[1]*Technische Universität Darmstadt, D-64289 Darmstadt, Germany*
[2]*Forschungszentrum Dresden-Rossendorf, P.O. Box 510119, D-01314 Dresden, Germany*
(Received 6 June 2008; revised manuscript received 3 September 2008; published 20 January 2009)

Using a homotopic family of boundary eigenvalue problems for the mean-field α^2 dynamo with helical turbulence parameter $\alpha(r)=\alpha_0+\gamma\Delta\alpha(r)$ and homotopy parameter $\beta\in[0,1]$, we show that the underlying network of diabolical points for Dirichlet (idealized, $\beta=0$) boundary conditions substantially determines the choreography of eigenvalues and thus the character of the dynamo instability for Robin (physically realistic, $\beta=1$) boundary conditions. In the (α_0,β,γ) space the Arnold tongues of oscillatory solutions at $\beta=1$ end up at the diabolical points for $\beta=0$. In the vicinity of the diabolical points the space orientation of the three-dimensional tongues, which are cones in first-order approximation, is determined by the Krein signature of the modes involved in the diabolical crossings at the apexes of the cones. The Krein space-induced geometry of the resonance zones explains the subtleties in finding α profiles leading to spectral exceptional points, which are important ingredients in recent theories of polarity reversals of the geomagnetic field.

DOI: 10.1103/PhysRevE.79.016205 PACS number(s): 05.45.−a, 91.25.Mf, 02.30.Tb, 02.40.Xx

I. INTRODUCTION

Polarity reversals of the Earth's magnetic field have fascinated geophysicists since their discovery by David and Brunhes [1] a century ago. While the last reversal occurred approximately 780 000 years ago, the mean reversal rate (averaged over the last few million years) is approximately 4 per million years. At least two, but very likely three [2], superchrons have been identified as "quiet" periods of some tens of millions of years showing no reversal at all.

The reality of reversals is quite complex and there is little hope to understand all their details within a simple model. Recent computer simulations of the geodynamo, in general and of reversals, in particular [3–5], have progressed much since the first fully coupled three-dimensional (3D) simulations of a reversal by Glatzmaier and Roberts in 1995 [6]. Most interestingly, polarity reversals were also observed in one [7] of the recent liquid sodium dynamo experiments, which have flourished during the last decade [8,9].

However, it is important to note that neither in simulations nor in experiments is it possible to accommodate all dimensionless parameters of the geodynamo [10], and many of them are not even well known [11]. In an interesting attempt to bridge the gap of several orders of magnitude between realistic and numerically achievable parameters, Christensen and Aubert [12] were able to identify remarkable scaling laws for some appropriate nondimensional numbers.

The use of appropriate simplified models [13–16] represents another attempt to understand better the basic principle and the typical features of reversals. Most prominent among those features are the distinct asymmetry (with a slow decay and a fast recovery phase) [17], the clustering property of reversal events [18], and the appearance of several maxima (at multiples of 95 000 years) of the residence time distribution, which has been explained in terms of a stochastic resonance phenonemon with the Milankovic cycle of the Earth's orbit eccentricity [19,20].

One of the simplest reversal models, which seems capable of explaining all those three reversal features in a consistent manner [21,22], relies basically on the existence of an exceptional point in the spectrum of the non-self-adjoint dynamo operator, where two real eigenvalues coalesce and continue as a complex conjugated pair of eigenvalues. The importance of the specific interplay between oscillatory and nonoscillatory modes for the reversal mechanism had been earlier expressed by Yoshimura [23], Sarson and Jones [24], and Gubbins and Gibbons [25]. In the framework of a simple mean-field α^2 dynamo with a spherically symmetric helical turbulence parameter α it was possible to identify reversals as noise-triggered relaxation oscillations in the vicinity of an exceptional point [26–28]. The key point is that the exceptional point is associated with a nearby local maximum of the growth rate situated at a slightly lower magnetic Reynolds number. It is the negative slope of the growth rate curve between this local maximum and the exceptional point that makes stationary dynamos vulnerable to noise. Then, the instantaneous eigenvalue is driven toward the exceptional point and beyond into the oscillatory branch where the sign change of the dipole polarity happens. Therefore, the existence of an exceptional point is an essential ingredient for reversals, although nonlinear dynamics and the influence of noise must be invoked for a more detailed understanding of those events.

From the spectral point of view, the reversal phenomenon of the geomagnetic field is strongly linked to other fields of physics, such as van der Pol-like oscillators [29], geometric phases [30], $\mathcal{PT}$-symmetric quantum mechanics [31,32], $\mathcal{PT}$-symmetric optical waveguides [33], microwave resonators [34], and dissipation-induced instabilities [35–37].

A particular problem of all those systems in which exceptional points are involved is a strong sensitivity of the eigenvalues on boundary conditions (BCs). As for the geodynamo, the periodic occurrence of so-called superchrons is usually attributed to the changing thermal BCs at the core-mantle

*kirillov@dyn.tu-darmstadt.de
†u.guenther@fzd.de
‡f.stefani@fzd.de

boundary [2], but the growth of the inner core may also play a role [28] by virtue of a spectral resonance phenomenon [38].

In this context it is worthwhile to note that important features of dynamos are most easily understandable when treated with idealized (i.e., nonphysical) boundary conditions. This was the case for explaining the famous eigenvalue symmetry between dipole and quadrupole modes as it was done by Proctor in 1977 [39,40].

Standing in this tradition, the present paper is devoted to a better understanding of the interplay of BCs, the spectral resonance phenomenon, and oscillatory regimes in dynamos.

II. MATHEMATICAL SETTING

The mean-field magnetohydrodynamic (MHD) α^2 dynamo [41] in its kinematic regime is described by a *linear* induction equation for the magnetic field. For spherically symmetric α profiles $\alpha(r)$ the vector of the magnetic field is decomposed into poloidal and toroidal components and expanded in spherical harmonics with degree l and order m. After additional time separation, the induction equation reduces to a set of l-decoupled boundary eigenvalue problems [38], which we write in a matrix form, convenient for the implementation of the perturbation theory [42,43]

$$\mathbf{Lf} := \mathbf{l}_0\partial_r^2\mathbf{f} + \mathbf{l}_1\partial_r\mathbf{f} + \mathbf{l}_2\mathbf{f} = 0, \quad \mathfrak{U}\mathfrak{f} = 0. \tag{1}$$

The matrices in the differential expression $\mathbf{L}$ are

$$\mathbf{l}_0 = \begin{pmatrix} 1 & 0 \\ -\alpha(r) & 1 \end{pmatrix}, \quad \mathbf{l}_1 = \partial_r\mathbf{l}_0,$$

$$\mathbf{l}_2 = \begin{pmatrix} -\dfrac{l(l+1)}{r^2} - \lambda & \alpha(r) \\ \alpha(r)\dfrac{l(l+1)}{r^2} & -\dfrac{l(l+1)}{r^2} - \lambda \end{pmatrix}, \tag{2}$$

and $\mathfrak{U} := [\mathfrak{A}, \mathfrak{B}] \in \mathbb{C}^{4\times 8}$ in the BCs consists of the blocks

$$\mathfrak{A} = \begin{pmatrix} 1 & 0 & 0 & 0 \\ 0 & 1 & 0 & 0 \\ 0 & 0 & 0 & 0 \\ 0 & 0 & 0 & 0 \end{pmatrix}, \quad \mathfrak{B} = \begin{pmatrix} 0 & 0 & 0 & 0 \\ 0 & 0 & 0 & 0 \\ \beta l + 1 - \beta & 0 & \beta & 0 \\ 0 & 1 & 0 & 0 \end{pmatrix}. \tag{3}$$

The vector function $\mathbf{f} \in \tilde{\mathcal{H}} = L_2(0,1) \oplus L_2(0,1)$ lives in the Hilbert space $(\tilde{\mathcal{H}}, (\ ,\ ))$ with inner product $(\mathbf{f},\mathbf{g}) = \int_0^1 \bar{\mathbf{g}}^T\mathbf{f}dr$, where the overbar denotes complex conjugation, and the boundary vector $\mathfrak{f}$ is given as

$$\mathfrak{f}^T := (\mathbf{f}^T(0), \partial_r\mathbf{f}^T(0), \mathbf{f}^T(1), \partial_r\mathbf{f}^T(1)) \in \mathbb{C}^8. \tag{4}$$

We assume that $\alpha(r) := \alpha_0 + \gamma\Delta\alpha(r)$, where $\Delta\alpha(r)$ is a smooth real function with $\int_0^1 \Delta\alpha(r)dr = 0$. For a fixed $\Delta\alpha(r)$ the differential expression $\mathbf{L}$ depends on the parameters α_0 and γ, while β interpolates between idealized ($\beta=0$) BCs, corresponding to an infinitely conducting exterior, and physically realistic ones ($\beta=1$) corresponding to a nonconducting exterior of the dynamo region [41].

The spectral problem (1) is not self-adjoint in a Hilbert space, but in the case of idealized BCs ($\beta=0$) the fundamental symmetry of the differential expression [38,44]

$$\mathbf{L}_0 := \mathbf{L}(\lambda = 0) = \mathbf{J}\mathbf{L}_0^\dagger\mathbf{J}, \quad \mathbf{J} = \begin{pmatrix} 0 & 1 \\ 1 & 0 \end{pmatrix} \tag{5}$$

makes $\mathbf{L}_0$ self-adjoint in a Krein space $(\mathcal{K}, [\ ,\ ])$ [45] with indefinite inner product $[\ ,\ ] = (\mathbf{J}\ ,\ )$:

$$[\mathbf{L}_0\mathbf{f},\mathbf{g}] = [\mathbf{f},\mathbf{L}_0\mathbf{g}], \quad \mathbf{f},\mathbf{g} \in \mathcal{K}. \tag{6}$$

For $\beta \neq 0$ the operator $\mathbf{L}_0$ is not self-adjoint even in a Krein space.

III. FROM DIABOLIC TO EXCEPTIONAL POINTS

In the case of constant α profiles $\alpha(r) \equiv \alpha_0 = \text{const}$ and $\beta = 0$ the spectrum and the eigenvectors of the operator matrix $\mathbf{L}_0$ are [38]

$$\lambda_n^\varepsilon = \lambda_n^\varepsilon(\alpha_0) = -\rho_n + \varepsilon\alpha_0\sqrt{\rho_n} \in \mathbb{R}, \quad \varepsilon = \pm,$$

$$\mathbf{f}_n^\varepsilon = \begin{pmatrix} 1 \\ \varepsilon\sqrt{\rho_n} \end{pmatrix} f_n \in \mathbb{R}^2 \otimes L_2(0,1), \quad n \in \mathbb{Z}^+, \tag{7}$$

with $f_n(r)$ being normalized Riccati-Bessel functions

$$f_n(r) = \frac{(2r)^{1/2} J_{l+(1/2)}(\sqrt{\rho_n}r)}{|J_{l+(3/2)}(\sqrt{\rho_n})|}, \quad (f_{n'}, f_n) = \delta_{n'n}, \tag{8}$$

and $\rho_n > 0$ the squares of Bessel function zeros

$$J_{l+(1/2)}(\sqrt{\rho_n}) = 0, \quad 0 < \sqrt{\rho_1} < \sqrt{\rho_2} < \cdots. \tag{9}$$

The eigenvectors $\mathbf{f}_n^+, \mathbf{f}_n^- \in \mathcal{K}_\pm \subset \mathcal{K}$ correspond to Krein space states of positive and negative signature $\varepsilon = \pm$,

$$[\mathbf{f}_{n'}^\pm, \mathbf{f}_n^\pm] = \pm 2\sqrt{\rho_n}\delta_{n'n}, \quad [\mathbf{f}_{n'}^\pm, \mathbf{f}_n^\mp] = 0. \tag{10}$$

The spectral branches $\lambda_n^\pm$ are real-valued linear functions of the parameter α_0 with signature-defined slopes $\pm\sqrt{\rho_n}$ and form for all $l = 0,1,2,\ldots$ a meshlike structure in the $(\alpha_0, \mathrm{Re}\,\lambda)$ plane. Spectral meshes for neighboring mode numbers l and $l+1$ have only slightly different slopes of their branches and behave qualitatively similar under perturbations [38]. Therefore basic spectral structures for $l = 1,2$ dipole and quadrupole modes can be illustrated by the simpler but unphysical $l=0$ monopole modes, which are given in terms of trigonometric functions. The ($l=0$) mesh built from $\rho_n = \pi^2 n^2$ is depicted as pink lines in Fig. 1.

The intersection of two branches $\lambda_{n'}^\delta, \lambda_n^\varepsilon$ with $n \neq n'$ occurs at points $(\alpha_0^{(\nu)}, \lambda^{(\nu)})$ with

$$\alpha_0^{(\nu)} := \varepsilon\sqrt{\rho_n} + \delta\sqrt{\rho_{n'}}, \quad \lambda^{(\nu)} := \sigma^{(\nu)}\sqrt{\rho_n\rho_{n'}}, \quad \sigma^{(\nu)} := \varepsilon\delta, \tag{11}$$

and corresponds to double eigenvalues $\lambda^{(\nu)} = \lambda_n^\varepsilon = \lambda_{n'}^\delta$ with two linearly independent eigenvectors $\mathbf{f}_n^\varepsilon$ and $\mathbf{f}_{n'}^\delta$, i.e., to so-called semisimple eigenvalues [diabolical points (DPs)] of algebraic and geometric multiplicity two [38,43].

For the $(l=0)$ mesh the diabolical crossings of the (εn)th and $(\varepsilon n+j)$th modes with the same fixed $|j| \in \mathbb{Z}^+$ are located on a parabolic curve [38]

$$\lambda(\alpha_0) = \frac{1}{4}(\alpha_0^2 - \pi^2 j^2), \tag{12}$$

where $\alpha_0 = \alpha_0^{(\nu)} = \pi(2n\varepsilon + j)$ and $\lambda^{(\nu)} = \lambda(\alpha_0^{(\nu)}) = \pi^2 n(n+\varepsilon j)$. Open circles in Figs. 1(a) and 1(b) indicate DPs on the parabolas $|j|=2$ and $|j|=4$. The Krein signatures [46] of the intersecting branches define the intersection index $\sigma^{(\nu)} = \varepsilon\delta = \mathrm{sgn}(\lambda^{(\nu)})$ in Eqs. (11). Branches of different signature $\delta \neq \varepsilon$ intersect for both signs of α_0 at $\lambda^{(\nu)} < 0$ (green circles in Fig. 1), whereas intersections at $\lambda^{(\nu)} > 0$ are induced by spectral branches of coinciding signatures: for $\varepsilon = \delta = +$ at $\alpha_0 > 0$, and for $\varepsilon = \delta = -$ at $\alpha_0 < 0$ (blue circles in Fig. 1).

For $\gamma=0$ and constant $\alpha(r)=\alpha_0$, the spectrum remains purely real on the full homotopic family $\beta \in [0,1]$ and passes smoothly in the $(\alpha_0, \mathrm{Re}\,\lambda)$ plane from the spectral mesh at $\beta=0$ to nonintersecting branches of simple real eigenvalues for models with physically realistic BCs at $\beta=1$. For the monopole model $l=0$ the full spectral homotopy is described by the characteristic equation $(1-\beta)\eta[\cos(\eta) - \cos(\alpha_0)] + 2\beta\lambda \sin(\eta) = 0$, where $\eta(\alpha_0,\lambda) = \sqrt{\alpha_0^2 - 4\lambda}$, which for physically realistic BCs $(\beta=1)$ leads to a spectrum consisting of the countably infinite set of parabolas (12) labeled by the index $j \in \mathbb{Z}^+$ and depicted in Fig. 1 as dashed lines. The reason for the $(\beta=0)$ DPs (11) to be located on the $(\beta=1)$ parabolas (12) is that the loci of the DPs are fixed points of the homotopy $\forall\, \beta \in [0,1]$—a phenomenon that is indicating on their "deep imprint" in the boundary eigenvalue problem (1).

The eigenvalue branches with $\mathrm{Re}\,\lambda > 0$, $\mathrm{Im}\,\lambda \neq 0$ (important for the reversal mechanism [26,28]) can be induced by deforming the constant α profile into an inhomogeneous one, $\alpha(r) = \alpha_0 + \gamma\Delta\alpha(r)$, with simultaneous variation of the BCs. This process is governed by a strong resonant correlation between the Fourier mode number of the inhomogeneous $\Delta\alpha(r)$ and the parabola index $|j|$. This is numerically demonstrated in Fig. 1 (black branches) for $\Delta\alpha(r) = \cos(2\pi k r)$, which highly selectively induces complex eigenvalue segments in the vicinity of DPs located on the parabola (12) with index $j=2k$.

The underlying influence of "hidden" DPs on real-to-complex transitions of the spectral branches can be made transparent by analyzing the perturbative unfolding of the DPs [43] at the mesh nodes $(\alpha_0^{(\nu)}, \lambda^{(\nu)})$ under variation of the parameters α_0, β, and γ. In first-order approximation this gives for the $(l=0)$ model

$$\lambda = \lambda^{(\nu)} - \lambda^{(\nu)}\beta + \frac{\alpha_0^{(\nu)}}{2}(\alpha_0 - \alpha_0^{(\nu)}) \pm \frac{\pi}{2}\sqrt{D}, \tag{13}$$

where $\alpha_0^{(\nu)} = \pi(\varepsilon n + \delta n')$, $\lambda^{(\nu)} = \varepsilon\delta\pi^2 n' n$, and

$$\begin{aligned} D := {} & [(\varepsilon n - \delta n')(\alpha_0 - \alpha_0^{(\nu)})]^2 + n'n[(\varepsilon 1 + \delta 1)\gamma A \\ & - (-1)^{n+n'}(n+n')\beta\pi]^2 - n'n[(\varepsilon 1 - \delta 1)\gamma A \\ & - (-1)^{n-n'}(n-n')\beta\pi]^2, \end{aligned} \tag{14}$$

with $A := \int_0^1 \Delta\alpha(r)\cos[(\varepsilon n - \delta n')\pi r]dr$.

For $\gamma=0$ it holds $D \geqslant 0$, confirming that the eigenvalues remain real under variation of the parameters α_0 and β only. If, additionally, $\alpha_0 = \alpha_0^{\nu}$, then one of the two simple eigenvalues (13) remains fixed under first-order perturbations with respect to β: $\lambda = \lambda^{(\nu)}$ in full accordance with the fixed point nature of the DP loci under the β homotopy. The sign of the first-order increment of the other eigenvalue $\lambda = \lambda^{(\nu)} - 2\lambda^{(\nu)}\beta$ depends on the sign of $\lambda^{(\nu)}$ and, therefore, via Eqs. (11) directly on the Krein signature of the modes involved in the crossing $(\alpha_0^{(\nu)}, \lambda^{(\nu)})$.

In general, there exist parameter combinations yielding $D<0$ and thus creating complex eigenvalues. Equation (14) implies that in first-order approximation the domain of oscillatory solutions with $\mathrm{Re}\,\lambda \neq 0$ and $\mathrm{Im}\,\lambda \neq 0$ in the $(\alpha_0, \beta, \gamma)$ space is bounded by the conical surfaces $D=0$ with apexes at the DPs $(\alpha_0^{(\nu)}, 0, 0)$, as shown in Fig. 2. Such domains, especially in the case of r-periodic α profiles, are in fact Arnold tongues corresponding to zones of parametric resonance [46] in Mathieu-type equations whose analysis in [47] was motivated just by Zeldovich's studies on MHD dynamos.

At the boundary $D=0$ the eigenvalues are twofold degenerate and nonderogatory; that is, they have Jordan chains consisting of an eigenvector and an associated vector. Thus, DPs in the $(\alpha_0, \beta, \gamma)$ space unfold into 3D conical surfaces consisting of exceptional points (EPs).

The conical zones develop according to resonance selection rules similar to those discovered in [38] for the case $\beta=0$. For example, with $\Delta\alpha(r) = \cos(2\pi k r)$, $k \in \mathbb{Z}$, the constant A in Eq. (14) yields

$$A = \begin{cases} 1/2, & 2k = \varepsilon n - \delta n', \\ 0, & 2k \neq \varepsilon n - \delta n', \end{cases} \tag{15}$$

so that in first-order approximation only DPs located on the $(j=2|k|)$ parabola (12) show a DP-EP unfolding (in accordance with numerical results in Fig. 1). The cone apexes correspond to $2|k|-1$ DPs with negative intersection index (11) $\sigma^{(\nu)} = -$ and countably infinite DPs with $\sigma^{(\nu)} = +$. The two groups are shown in Fig. 2 in green and blue, respectively.

The real parts of the perturbed eigenvalues are given by $\mathrm{Re}\,\lambda = \lambda^{(\nu)}(1-\beta) + \alpha_0^{(\nu)}(\alpha_0 - \alpha_0^{(\nu)})/2$ and for fixed α_0 and increasing β they are shifted (for both groups) away from the original DP positions toward the $(\mathrm{Re}\,\lambda = 0)$ axis (cf. the numerical results in Fig. 1)—an effect that is similar to the self-tuning mechanism of field reversals uncovered in [26].

Apart from this similarity, the eigenvalues of the two cone groups show significant differences. The $2|k|-1$ cones of the first group have nontrivial intersection with the plane $\beta=0$. In this (α_0, γ) plane the zones of decaying oscillatory modes are $\gamma \rightleftharpoons -\gamma$ symmetric and defined by the inequality

$$[\alpha_0 \pm 2\pi(n - |k|)]^2 < \frac{\gamma^2}{4}\left[1 - \left(\frac{n-|k|}{|k|}\right)^2\right], \tag{16}$$

where $n = 1, 2, \ldots, |k|$. For $k=2$ there are three primary Arnold tongues: $4\alpha_0^2 < \gamma^2$ and $16(\alpha_0 \pm 2\pi)^2 < 3\gamma^2$.

The cones of the second group meet the plane $\beta=0$ only at the apexes, having their skirts located in the sectors $[\beta > 0, \gamma\,\mathrm{sgn}(\alpha_0) > 0]$ and $[\beta < 0, \gamma\,\mathrm{sgn}(\alpha_0) < 0]$ [cf. Fig. 2(b)].

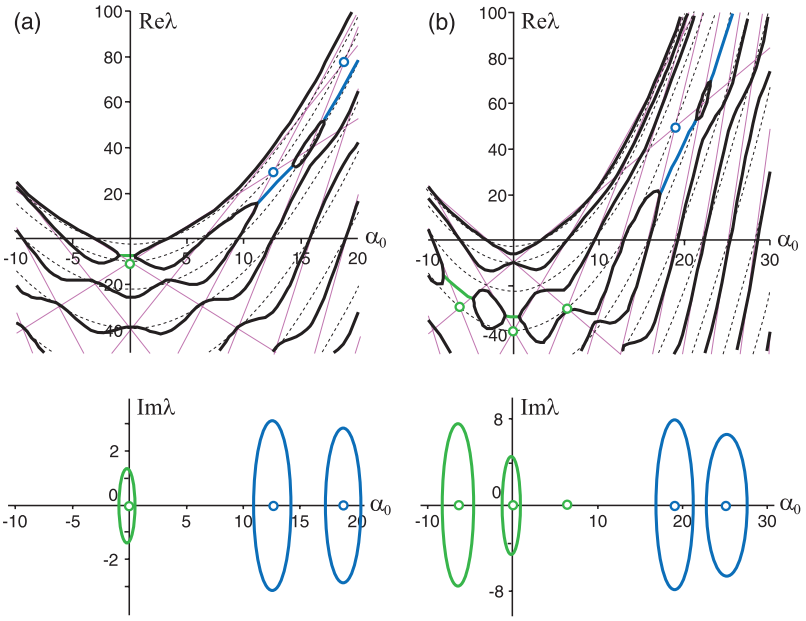

FIG. 1. (Color) $l=0$: (Pink) Spectral mesh (11) for $\gamma=0$, $\beta=0$; (dashed) eigenvalue parabolas (12) for $\gamma=0$, $\beta=1$; (black) eigenvalue branches for $\beta=0.3$, $\Delta\alpha(r)=\cos(2\pi kr)$, and (a) $k=1$, $\gamma=2.5$, (b) $k=2$, $\gamma=3$, with resonant overlaps near the locations of the diabolically crossed modes having (blue) the same and (green) different Krein signature.

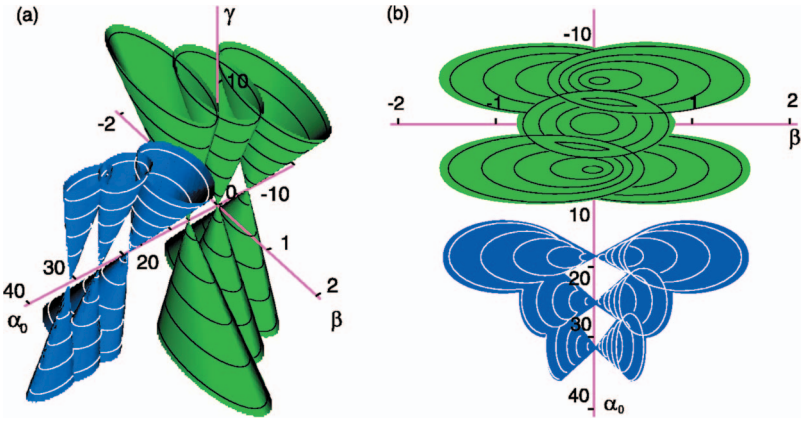

FIG. 2. (Color) $l=0$, $\Delta\alpha(r)=\cos(4\pi r)$: (a) Linear approximation of the 3D Arnold tongues and (b) their projection onto the (α_0,β) plane indicating the influence of the intersection index $\sigma^{(\nu)}$ on the inclination of the cones.

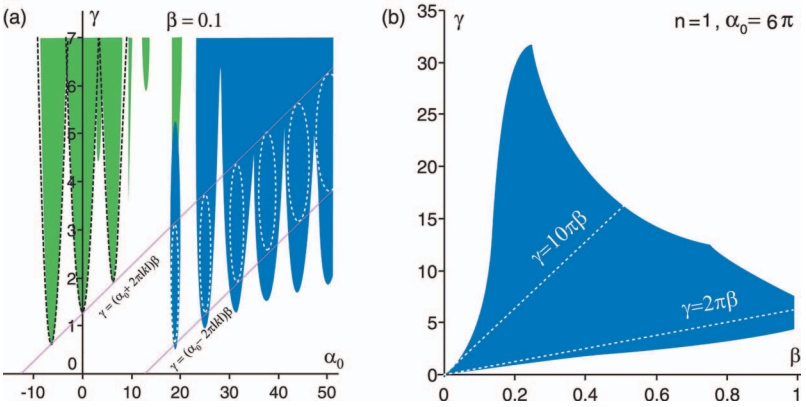

FIG. 3. (Color) $l=0$: Numerically calculated Arnold tongues for $\Delta\alpha(r)=\cos(2\pi kr)$, $k=2$, and $\lambda^{(\nu)}<0$ (green) or $\lambda^{(\nu)}>0$ (blue) and their approximations (dashed lines) (a) in the (α_0,γ) plane and (b) in the (β,γ) plane.

Therefore, in models with idealized BCs ($\beta=0$) complex eigenvalues occur only in zones (16) in the (α_0,γ) plane.

The different oscillatory behavior induced by the two cone groups has its origin in the different Krein-signature-defined inclination of the $(D<0)$ cones with respect to the $(\beta=0)$ plane.

Passing from $\beta=0$ to a parallel $(\beta\neq 0)$ plane, the $(D<0)$ tongues (16), corresponding to $\lambda^{(\nu)}<0$, deform into cross sections bounded by hyperbolic curves [black dashed lines in Fig. 3(a)]

$$-4k^2[\alpha_0 \pm 2\pi(n-|k|)]^2 + n(2|k|-n)[\gamma \pm 2\pi(n-|k|)\beta]^2 > n(2|k|-n)4\pi^2\beta^2k^2, \quad (17)$$

with $n=1,2,\ldots,|k|$. Since $n\leqslant|k|$, the lines $\gamma=\pm 2\pi n\beta$ and $\gamma=\pm 2\pi(n-2|k|)\beta$, bounding the cross sections of the 3D cones by the plane $\alpha_0=\pm 2\pi(n-|k|)$, always have the slopes of different sign. This allows decaying oscillatory modes for $\beta=0$ due to variation of γ only.

The $(\beta\neq 0)$ cross sections of the cones with $(\lambda^{(\nu)}>0)$ apexes have the form of ellipses [white dashed lines in Fig. 3(a)]

$$4k^2[\alpha_0 \pm 2\pi(n+|k|)]^2 + n(2|k|+n)[\gamma \pm 2\pi(n+|k|)\beta]^2 < n(2|k|+n)4\pi^2\beta^2k^2, \quad (18)$$

where $n=1,2,\ldots$. In the $(\beta\neq 0)$ plane the ellipses are located inside the stripe with boundaries $\gamma=(\alpha_0\pm 2\pi|k|)\beta$ [pink lines in Fig. 3(a)], while the hyperbolas lie outside this stripe. Moreover, since in the plane $\alpha_0=\pm 2\pi(n+|k|)$the boundary lines $\gamma=\pm 2\pi n\beta$ and $\gamma=\pm 2\pi(n+2|k|)\beta$ have slopes of the same sign, the γ axis does not belong to the instability domains, showing that for growing oscillatory modes the parameters β and γ have to be taken in a prescribed proportion [see Fig. 3(b)].

The amplitude γ of the inhomogeneous perturbation of the α profile $\gamma\Delta\alpha(r)$ is limited both from below and from above in the vicinity of the DPs with $\sigma^{(\nu)}>0$. However, numerical calculations indicate that this property can persist on the whole interval $\beta\in[0,1]$ [see Fig. 3(b)], in agreement with the earlier findings of [48].

IV. CONCLUSIONS

In summary, we have found that the underlying network of DPs and their intersection indices for $\beta=0$ substantially determine the choreography of eigenvalues for $\beta=1$ and, in particular, the loci of EPs, which are important to explain the reversals of the geomagnetic field. Although this has been exemplified for the unphysical monopole $(l=0)$ mode of a simplified spherically symmetric α^2 dynamo model, the general idea is well generalizable to physical modes and to more realistic dynamo models. Work in this direction is in progress.

ACKNOWLEDGMENTS

The research of O.N.K. was supported by DFG Grant No. HA 1060/43-1 as well as by the Saxon Ministry of Science Grant No. 4-7531.50-04-844-07/8 and that of U.G. and F.S. by DFG Sonderforschungsbereich 609.

[1] B. Brunhes, J. Phys. **5**, 705 (1906).
[2] V. Courtillot and P. Olson, Earth Planet. Sci. Lett. **260**, 495 (2007).
[3] G. A. Glatzmaier, Annu. Rev. Earth Planet Sci. **30**, 237 (2002).
[4] J. Wicht and P. Olson, Geochem., Geophys., Geosyst. **5**, Q03H10 (2004).
[5] F. Takahashi, M. Matsushima, and Y. Honkura, Science **309**, 459 (2005).
[6] G. A. Glatzmaier and P. H. Roberts, Nature (London) **377**, 203 (1995).
[7] M. Berhanu *et al.*, Europhys Lett **77**, 59001 (2007).
[8] A. Gailitis, O. Lielausis, E. Platacis, G. Gerbeth, and F. Stefani, Rev. Mod. Phys. **74**, 973 (2002).
[9] F. Stefani, A. Gailitis, and G. Gerbeth, Z. Angew. Math. Mech. **88**, 930 (2008).
[10] D. Gubbins, Nature (London) **452**, 165 (2008).
[11] P. H. Roberts and G. A. Glatzmaier, Rev. Mod. Phys. **72**, 1081 (2000).
[12] U. R. Christensen and J. Aubert, Geophys. J. Int. **166**, 97 (2006).
[13] I. Melbourne, M. R. E. Proctor, and A. M. Rucklidge, in *Dynamo and Dynamics, a Mathematical Challenge*, edited by P. Chossat, D. Armbruster, and I. Oprea (Kluwer, Dordrecht, 2001), pp. 363–370.
[14] P. Hoyng, M. A. J. H. Ossendrijver, and D. Schmidt, Geophys. Astrophys. Fluid Dyn. **94**, 263 (2001).
[15] D. A. Ryan and G. R. Sarson, Geophys. Res. Lett. **34**, L02307 (2007).
[16] L. Sorriso-Valvo *et al.*, Phys. Earth Planet. Inter. **164**, 197 (2007).
[17] J.-P. Valet, L. Meynadier, and Y. Guyodo, Nature (London) **435**, 802 (2005).
[18] V. Carbone, L. Sorriso-Valvo, A. Vecchio, F. Lepreti, P. Veltri, P. Harabaglia, and I. Guerra, Phys. Rev. Lett. **96**, 128501 (2006).
[19] G. Consolini and P. De Michelis, Phys. Rev. Lett. **90**, 058501 (2003).
[20] S. Lorito, D. Schmitt, G. Consolini, and P. De Michelis, Astron. Nachr. **326**, 227 (2005).
[21] M. Fischer, G. Gerbeth, and F. Stefani, Eur. Phys. J. B **65**, 547 (2008).
[22] M. Fischer, G. Gerbeth, A. Giesecke, and F. Stefani, e-print arXiv:0808.3310.
[23] H Yoshimura, Z. Wang, and F. Wu, Astrophys. J. **283**, 870 (1984).
[24] G. R. Sarson and C. A. Jones, Phys. Earth Planet. Inter. **111**, 3 (1999).
[25] D. Gubbins and S. Gibbons, Geophys. Astrophys. Fluid Dyn. **96**, 481 (2002).

[26] F. Stefani and G. Gerbeth, Phys. Rev. Lett. **94**, 184506 (2005).
[27] F. Stefani, G. Gerbeth, U. Günther, and M. Xu, Earth Planet. Sci. Lett. **243**, 828 (2006).
[28] F. Stefani, M. Xu, L. Sorriso-Valvo, and U. Günther, Geophys. Astrophys. Fluid Dyn. **101**, 227 (2007).
[29] B. van der Pol, Philos. Mag. **2**, 978 (1926).
[30] A. A. Mailybaev, O. N. Kirillov, and A. P. Seyranian, Phys. Rev. A **72**, 014104 (2005); U. Günther, I. Rotter, and B. Samsonov, J. Phys. A **40**, 8815 (2007).
[31] C. M. Bender and S. Boettcher, Phys. Rev. Lett. **80**, 5243 (1998); C. M. Bender, Rep. Prog. Phys. **70**, 947 (2007).
[32] E.-M. Graefe, U. Günther, H.-J. Korsch, and A. Niederle, J. Phys. A **41**, 255206 (2008).
[33] Z. H. Musslimani, K. G. Makris, R. El-Ganainy, and D. N. Christodoulides, Phys. Rev. Lett. **100**, 030402 (2008); K. G. Makris, R. El-Ganainy, D. N. Christodoulides, and Z. H. Musslimani, *ibid.* **100**, 103904 (2008); S. Klaiman, U. Günther, and N. Moiseyev, *ibid.* **101**, 080402 (2008).
[34] C. Dembowski, B. Dietz, H. D. Graf, H. L. Harney, A. Heine, W. D. Heiss, and A. Richter, Phys. Rev. Lett. **90**, 034101 (2003).
[35] O. Bottema, Indag. Math. **18**, 403 (1956).
[36] R. Krechetnikov and J. E. Marsden, Rev. Mod. Phys. **79**, 519 (2007); N. M. Bou-Rabee, J. E. Marsden, and L. A. Romero, SIAM Rev. **50**, 325 (2008).
[37] O. N. Kirillov, Acta Mech. **174**, 145 (2005); Int. J. Non-Linear Mech. **42**, 71 (2007); Proc. R. Soc. London, Ser. A **464**, 2321 (2008).
[38] U. Günther and O. N. Kirillov, J. Phys. A **39**, 10057 (2006).
[39] M. R. E. Proctor, Astron. Nachr. **298**, 19 (1977).
[40] M. R. E. Proctor, Geophys. Astrophys. Fluid Dyn. **8**, 311 (1977).
[41] F. Krause and K.-H. Rädler, *Mean-Field Magnetohydrodynamics and Dynamo Theory* (Akademie-Verlag, Berlin/Pergamon Press, Oxford, 1980), Chap. 14.
[42] M. I. Vishik and L. A. Lyusternik, Russ. Math. Surveys **15**, 1 (1960); J. Moro, J. V. Burke, and M. L. Overton, SIAM J. Matrix Anal. Appl. **18**, 793 (1997).
[43] O. N. Kirillov and A. P. Seyranian, SIAM J. Appl. Math. **64**, 1383 (2004); J. Appl. Math. Mech. **69**, 529 (2005); O. N. Kirillov, A. A. Mailybaev, and A. P. Seyranian, J. Phys. A **38**, 5531 (2005); O. N. Kirillov (to be published); e-print arXiv:0803.2248v2.
[44] U. Günther and F. Stefani, J. Math. Phys. **44**, 3097 (2003); U. Günther, F. Stefani, and M. Znojil, *ibid.* **46**, 063504 (2005); U. Günther, B. Samsonov, and F. Stefani, J. Phys. A **40**, F169 (2007).
[45] H. Langer and C. Tretter, Czech. J. Phys. **54**, 1113 (2004).
[46] M. G. Krein, Dokl. Akad. Nauk SSSR **73**, 445 (1950).
[47] V. I. Arnold, Usp. Mat. Nauk **38**, 189 (1983).
[48] F. Stefani and G. Gerbeth, Phys. Rev. E **67**, 027302 (2003).